4216 *Chem. Mater.* **2009,** *21,* 4216–4222
DOI:10.1021/cm900998n

CHEMISTRY OF MATERIALS
Article

Reinvestigation of Li_2MnO_3 Structure: Electron Diffraction and High Resolution TEM

A. Boulineau,[†,‡] L. Croguennec,[†,‡] C. Delmas,[†,‡] and F. Weill*[,†,‡,§]

[†]*CNRS, ICMCB, 87 avenue du Dr. A. Schweitzer, PESSAC, F-33608, France,* [‡]*Université de Bordeaux, ICMCB, ENSCPB, PESSAC, F-33608, France, and* [§]*Université de Bordeaux, CREMEM, TALENCE, F-33405, France*

Received April 10, 2009. Revised Manuscript Received July 24, 2009

The structure of Li_2MnO_3 was investigated by the means of X-ray and electron diffraction as well as high resolution transmission electron microscopy experiments. Extra spots are present in the Li_2MnO_3 electron diffraction patterns, and their origin is fully understood and explained here. They result from the existence of diffuse scattering lines observed along the *c** monoclinic axis, intercepted by the Ewald's sphere, and not from double diffraction phenomenon nor from superstructure. Furthermore, the origin of these scattering lines is due to stacking faults of the ordered lithium/manganese layers along the *c*-axis that were observed in images obtained using high resolution transmission electron microscopy.

1. Introduction

It has been shown during the last 20 years that $LiMO_2$ materials (M = Ni, Co, Mn, ...) with a two-dimensional layered structure are of high fundamental and technological interest as positive electrode materials for lithium-ion batteries.[1−5] More recently, manganese-rich materials such as $LiNi_{1/3}Mn_{1/3}Co_{1/3}O_2$ and $LiNi_{1/2}Mn_{1/2}O_2$ were shown to be good alternatives to $LiCoO_2$ [6,7] due to their high thermal stability in the charged state but also to their low cost. The presence of an in plane $\sqrt{3}a_{hex} \times \sqrt{3}a_{hex}$ superstructure was clearly established in these materials: it was shown to come from a cation ordering similar to that previously described for Li_2MnO_3. According to first-principles calculations,[8] Ozhuku's research group proposed for $LiNi_{1/3}Mn_{1/3}Co_{1/3}O_2$ a $[\sqrt{3}a_{hex} \times \sqrt{3}a_{hex}]$-type superstructure based on an α-$NaFeO_2$-type structure that was confirmed by electron diffraction.[9] Meng et al.[10] also showed the presence of such a superstructure in the transition metal layers of the material $LiNi_{0.5}Mn_{0.5}O_2$. Ngala et al. [11] pointed out that this order in the transition metal layers of these manganese rich materials like $LiNi_{1-y-z}Mn_yCo_zO_2$ decreases with increasing cobalt concentration and increases with increasing nickel concentration. Thackeray et al. proposed also the existence of ordered domains in materials like $Li_{1+x}[Ni_{0.5}Mn_{0.5}]_{1-x}O_2$ and $Li_{1+x}[Ni_{1/3}Mn_{1/3}Co_{1/3}]_{1-x}O_2$ with $0 < x < 0.15$ [12] and have highlighted in ref 13 the structural complexity of the materials they formulated $xLi_2MnO_3 \cdot (1 - x)LiMO_2$ (M = Mn, Ni, Co). Finally, some of us [14] have suggested by X-ray diffraction and confirmed by electron diffraction the presence of an in plane $\sqrt{3}a_{hex} \times \sqrt{3}a_{hex}$ superstructure in the transition metal layers of materials $Li_{1+x}[Ni_{0.425}Mn_{0.425}Co_{0.15}]_{1-x}O_2$ with $x = 0$ and 0.12. As shown by all these studies, the structures of these Mn-rich materials are complex and not yet fully understood.

Li_2MnO_3 can be considered as the simplest model for these tetravalent manganese-rich layered compounds regarding its chemical formula. The structure of Li_2MnO_3 is better described by the $Li[Li_{1/3}Mn_{2/3}]O_2$ formula in relation with its layered structure. It is an O3-type structure[15] where interslab octahedral sites are only occupied by lithium ions whereas slab octahedral sites are occupied by lithium and manganese ions with the (1:2) ratio. As a result of the differences in ionic radii between Li^+ and Mn^{4+} ions (0.74 and 0.54 Å, respectively[16]), they are

*Corresponding author. Phone: +33 (0)5 40 00 26 54. Fax: +33 (0)5 40 00 27 61. E-mail: weill@icmcb-bordeaux.cnrs.fr.

(1) Mizushima, K.; Jones, P. C.; Wiseman, P. J.; Goodenough, J. B. *Mater. Res. Bull.* **1980**, *15*, 783.
(2) Abe, H.; Zaghib, K.; Tatsumi, K.; Higuchi, S. *J. Power Sources* **1995**, *54*, 236.
(3) Ménétrier, M.; Saadoune, I.; Levasseur, S.; Delmas, C. *J. Mater. Chem.* **1999**, *9*, 1135.
(4) Weaving, J. S.; Coowar, F.; Teagle, D. A.; Cullen, J.; Dass, V.; Bindin, P.; Green, R.; Macklin, W. J. *J. Power Sources* **2001**, *97*, 733.
(5) Guilmard, M.; Pouillerie, C.; Croguennec, L.; Delmas, C. *Solid State Ionics* **2003**, *160*, 39.
(6) Ohzuku, T.; Makimura, Y. *Chem. Lett.* **2001**, 744.
(7) Ohzuku, T.; Makimura, Y. *Chem. Lett.* **2001**, 642.
(8) Koyama, Y.; Yabuuchi, N.; Tanaka, I.; Adachi, H.; Ozhuku, T. *J. Electrochem. Soc.* **2004**, *151*(10), A1545.
(9) Koyama, Y.; Yabuuchi, N.; Tanaka, I.; Adachi, H.; Ozhuku, T. *J. Electrochem. Soc.* **2005**, *152*(7), A1434.
(10) Meng, Y. S.; Ceder, G.; Grey, C. P.; Yoon, W.-S.; Shao Horn, Y. *Electrochem. Solid State Lett.* **2004**, *7*(6), A155.
(11) Ngala, J. K.; Chernova, N. A.; Ma, M.; Mamak, M.; Zavalija, P. Y.; Whittingham, M. S. *J. Mater. Chem.* **2004**, *14*, 214.
(12) Thackeray, M. M.; Kang, S. H.; Johnson, C. S.; Vaughey, J. T.; Hackney, S. A. *Electrochem. Commun.* **2006**, *8*, 1531.
(13) Thackeray, M. M.; Kang, S.-H.; Johnson, C. S.; Vaughey, J. T.; Benedek, R.; Hackney, S. A. *J. Mater. Chem.* **2007**, *17*, 3112.
(14) Weill, F.; Tran, N.; Croguennec, L.; Delmas, C. *J. Power Sources* **2007**, *172*, 893.
(15) Delmas, C.; Fouassier, C.; Hagenmuller, P. *Physica* **1980**, *99B*, 81.
(16) Shannon, R. D.; Prewitt, C. T. *Acta Crystallogr., B* **1969**, *25*, 925.

 Published on Web 08/27/2009

ordered in the slab according to a $\sqrt{3}a_{hex} \times \sqrt{3}a_{hex}$ superstructure to minimize the strains.

Li_2MnO_3 structure has been determined by Strobel et al. [17] using single crystal X-ray diffraction. The structure is described by the space group $C2/m$, in a monoclinic cell which parameters are $a_{mon.} = 4.937(1)$ Å, $b_{mon.} = 8.532(1)$ Å, $c_{mon.} = 5.030(2)$ Å, and $\beta = 109.46(3)°$. Lithium ions occupy the 2b (0, 1/2, 0), 2c (0, 0, 1/2), and 4h (0, 0.6606(3), 1/2) sites, the manganese ions the 4g (0, 0.16708(2), 0) site, and the oxygen ions the 4i (0.2189(2), 0, 0.2273(2)) and 8j (0.2540(1), 0.32119(7), 0.2233(1)) sites. The anisotropic thermal parameters of lithium in the 2b site could not be refined in this study.

However, controversies about the structure of Li_2MnO_3 exist in literature. Jansen et al. [18] and Riou et al. [19] proposed the $C2/c$ space group to describe its structure, but they did not take into account the presence of a mirror parallel to the *ac* plane in the cell. Massarotti et al. [20] confirmed the $C2/m$ space group as determined by Strobel et al. They found, as Strobel et al., a negative value for the isotropic displacement parameter of lithium ions on the 2b site suggesting a possible partial exchange between Mn and Li on the 4g and 2b sites, respectively. Moreover the observation of some inadequacies between the calculated X-ray diffraction profile and the experimental data was attributed to microstructural effects.

The stacking of the transition metal layers is also a subject of debate in literature. In fact, as described by Lang et al. [21] and then by Bréger et al.,[22] there are three ways, very closed in energy (1 or 2 meV of difference), to stack the honeycomb ordered $(Li_{1/3}Mn_{2/3})O_2$ layers, each stacking sequence being described by a different space group. Recently Meng et al., in Li_2MnO_3 crystals synthesized at 850 °C as in $LiNi_{0.5}Mn_{0.5}O_2$ [10,23], pointed out by transmission electron microscopy (TEM) the presence of a superstructure explained in the $P3_112$ space group, that describes a peculiar slabs stacking sequence. To explain their X-ray diffraction patterns, these authors consider the existence of intergrowths between the $C2/m$ structure and their $P3_112$ superstructure.

By means of X-ray and electron diffraction experiments we have reported in a previous article that it was not possible to synthesize the ideal compound, that is, free of stacking faults, either via "classical" coprecipitation or by solid state reaction syntheses.[24] Indeed, we have demonstrated that the ordered $(Li_{1/3}Mn_{2/3})$ planes are never perfectly stacked along the *c*-axis and that the distribution of these stacking faults is not strictly statistical. Furthermore, the numbers of stacking faults depends on the temperature of the thermal treatment used during the synthesis: the higher the temperature the lower is the number of stacking faults.

In this context, we undertook a new exploration of the structure of Li_2MnO_3, by means of X-ray and electron diffraction as well as high resolution transmission electron microscopy, to get a clear idea of the structure of this compound and a deep knowledge of the stacking faults.

2. Experimental Section

Li_2MnO_3 powder was prepared by a solid state synthesis performed according to ref 25 in two steps. The first one consisted in the addition of 5 g of $KMnO_4$ in 400 mL of distilled water with 5 mL of ethanol, maintained under stirring in a stainless steel autoclave at 100 °C during 24 h and led to the formation of nanometric particles of MnO(OH) powder material. The as-prepared manganese oxy-hydroxide was washed with distilled water and then with acetone and dried at 80 °C during about 60 h. A thermogravimetric analysis confirmed the actual composition of the material. In the second step, the obtained MnO(OH) powder was ground with an excess of LiOH (molar ratio Li/Mn = 2.1) to compensate for the lithium loss during the annealing treatment in air at 900 °C for 4 h. Finally, the average oxidation state of manganese in the prepared Li_2MnO_3 powder was determined by iodometric back-titration. The Li/Mn ratio was measured using an ICP-OES apparatus (Varian 720-ES) after the complete dissolution of the powder into acidic solution.

The XRD pattern of the as prepared Li_2MnO_3 powder was collected at room temperature using a Siemens D5000 powder diffractometer in the Bragg−Brentano $\theta-\theta$ geometry with a back monochromator, using the Cu Kα radiation. The data were recorded in the 10−120° 2θ range in step of 0.02° (2θ) with a constant counting time of 45 s. The pattern was analyzed by Rietveld refinement as implemented in the program Fullprof.[26]

Electron diffraction experiments and high resolution images were performed respectively with a JEOL 2000FX and a JEOL 2200FS microscopes equipped with double tilt specimen holders. Both were used at an accelerating voltage of 200 kV. The powder was ground in ethanol, and a droplet of this suspension was then deposited on a lacey carbon grid. Electron diffraction experiments were carried out on many crystallites, and very reproducible results were observed. The particles studied were chosen as isolated as possible and as thin as possible. High resolution images were simulated with JEMS software developed by P. Stadelmann using the multislice method.

3. Results and Discussion

3.1. Chemical Analysis, X-ray Powder Diffraction, and Structure Analysis Using the Rietveld Refinement Method. The Li/Mn ratio and the oxidation state of manganese were found to be 1.96 and 3.85, respectively, leading thus to the chemical composition $Li_{1.96(3)}MnO_{2.91(3)}$. In a previous study [24] we have shown that, among a series of compounds, the synthesis conditions we used in the present study lead to the formation of the Li_2MnO_3 type

(17) Strobel, P.; Lambert-Andron, B. *J. Solid State Chem.* **1988**, *75*, 90.
(18) Jansen, V.; Hoppe, R. *Z. Anorg. Allg. Chem.* **1973**, *397*, 279.
(19) Riou, A.; Lecerf, A.; Gerault, Y.; Cudennec, Y. *Mater. Res. Bull.* **1992**, *27*, 269.
(20) Massarotti, V.; Bini, M.; Capsoni, D.; Altomare, A.; Moliterni, A. G. G. *J. Appl. Crystallogr.* **1997**, *30*, 123.
(21) Lang, G. *Z. Anorg. Allg. Chem.* **1966**, *348*, 246.
(22) Bréger, J.; Jiang, M.; Dupré, N.; Meng, Y. S.; Shao-Horn, Y.; Ceder, G.; Grey, C. P. *J. Solid State Chem.* **2005**, *178*, 2575.
(23) Meng, Y. S.; Ceder, G.; Grey, C. P.; Yoon, W.-S.; Jiang, M.; Bréger, J.; Shao Horn, Y. *Chem. Mater.* **2005**, *17*, 2386.
(24) Boulineau, A.; Croguennec, L.; Delmas, C.; Weill, F. *Solid State Ionics*, accepted.
(25) Zhang, W.; Liu, Y.; Yang, Z.; Tang, S.; Chen, M. *Solid State Commun.* **2004**, *131*, 441.
(26) Rodriguez-Carvajal, J. XV Congress of Int. Union of Crystallography, Satellite Meeting on Powder Diffraction 127, **1990** (http://www.ill.eu/sites/fullprof/).

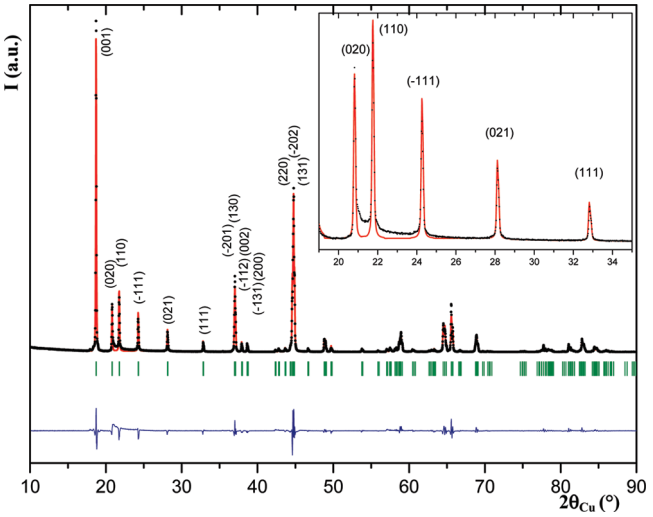

Figure 1. Rietveld plot of the as prepared Li_2MnO_3 sample. Detail of the reflections related to the Li/Mn ordering in the slabs is given in insert. The 90−120° (2θ) range is not presented to enlarge the figure.

material that presents the X-ray diffraction pattern the closest to the theoretical one in spite of a slight nonstoichiometry.

The X-ray diffraction pattern that is given in Figure 1 was refined according to the procedure described in ref 24. We considered possible Li/Mn exchange between the 2b and 4g sites in the slab in accordance with the formula $\{(Li_2)_{2c}(Li_4)_{4h}\}_{interslab}\{(Li_{2-z}Mn_z)_{2b}(Mn_{4-z}Li_z)_{4g}\}_{slab}(O_{12})_{4i,8j}$, the four cations crystallographic sites being fully occupied. The lithium isotropic atomic thermal displacement parameters (B_{iso}) were fixed to 1.0 Å^2, the manganese one to 0.5 Å^2, and the oxygen one to 0.8 Å^2. This refinement revealed cell parameters (a = 4.9292(2) Å, b = 8.5315(2) Å, c = 5.0251(1) Å, β = 109.337(2)°) and structural parameters very close to those reported by Strobel et al. [17] and that about 0.29 ions are exchanged between the Mn 4g and Li 2b sites in the slabs leading to the crystallographic formula $\{(Li_2)_{2c}(Li_4)_{4h}\}_{interslab}\{(Li_{1.71}Mn_{0.29})_{2b}(Mn_{3.71}Li_{0.29})_{4g}\}_{slab}(O_{12})_{4i,8j}$ (see Table S1 given in Supporting Information).

Despite a rather good minimization of the difference between the observed and the calculated intensities, the fit to the profile and the reliability factors remain rather poor (R_{wp} = 27.8%, R_{Bragg} = 7.8%, and S_{cor} = 2.99). This is due to different profiles for the reflections and especially to a huge broadening of the bottom of the (020) and (110) peaks as shown in inset in Figure 1. As previously reported by other authors, this broadening could be attributed to the existence of structural defects (strains or size effects) [20] or faults in the stacking of the ordered cationic layers along the c monoclinic axis.[17,22] In a previous article,[24] we have shown using X-ray diffraction patterns simulation that stacking faults had indeed to be considered to explain the profile of the reflections of the X-ray diffraction pattern corresponding to the Li/Mn ordering.

3.2. Electron Diffraction Study. A series of nine electron diffraction patterns collected from the same Li_2MnO_3 crystal is presented in Figure 2. The first five patterns were obtained by rotation around the [001]* axis, and the last four were collected from the fifth by tilting around the direction [3$\bar{3}\bar{1}$]*, which is almost perpendicular to [001]*. Note that this series of patterns is representative of all the crystals studied.

Table 1. Correspondence between the Two Indexations of Some of the Planes Experimentally Observed

plane indexation in the $C2/m$ space group	plane indexation in the $R\bar{3}m$ space group
001	003
310	not indexable
200	$\bar{1}02$
3$\bar{1}$0	not indexable
33$\bar{1}$	$\bar{2}10$
22$\bar{1}$	not indexable

The first five patterns are essential to understand the crystallography of such a material. Note that all the reflections appearing on these patterns can be fully indexed using the $C2/m$ space group. Also, on all the patterns containing the c* direction except in the [010] zone axis one, diffuse scattering lines can be observed. They are located along reciprocal directions parallel to the [001]* axis. The location of these scattering lines is particular; diffusion is not localized on all the rows as evidenced on the [010] and [110] zone axis experimental patterns. Their three-dimensional arrangement is represented in Figure 3. To understand this feature it is necessary to come back to the relation between this structure described in the $C2/m$ space group and the parent trigonal ($R\bar{3}m$) structure related to the α-$NaFeO_2$ phase. The monoclinic cell is deduced from the parent trigonal one (in a hexagonal setting) using the relation

$$(\vec{a}\quad\vec{b}\quad\vec{c})_{mon.} = (\vec{a}\quad\vec{b}\quad\vec{c})_{trig.}\begin{pmatrix} -2 & 0 & 2/3 \\ -1 & -3 & 1/3 \\ 0 & 0 & 1/3 \end{pmatrix}$$

Then, the indexation of the experimental patterns using the parent trigonal symmetry (in a hexagonal setting) can be deduced using the relation

$$(h\quad k\quad l)_{trig.} = (h\quad k\quad l)_{mon.}\begin{pmatrix} -1/2 & 0 & 1 \\ 1/6 & -1/3 & 0 \\ 0 & 0 & 3 \end{pmatrix}$$

Table 1 presents the correspondence between the two indexations of some of the planes experimentally observed. Some monoclinic indexations do not have any correspondence in the trigonal cell related to the α-$NaFeO_2$ phase. This further demonstrates the need to use the monoclinic cell to explain the patterns. Furthermore, the reflections not indexable in the trigonal cell are always associated with diffusion lines parallel to the c* direction, whereas when a trigonal correspondence does exist, no diffuse scattering lines running through the corresponding reflection are observed.

As diffusion is present (i) along directions parallel to [001]* and (ii) only between reflections corresponding to

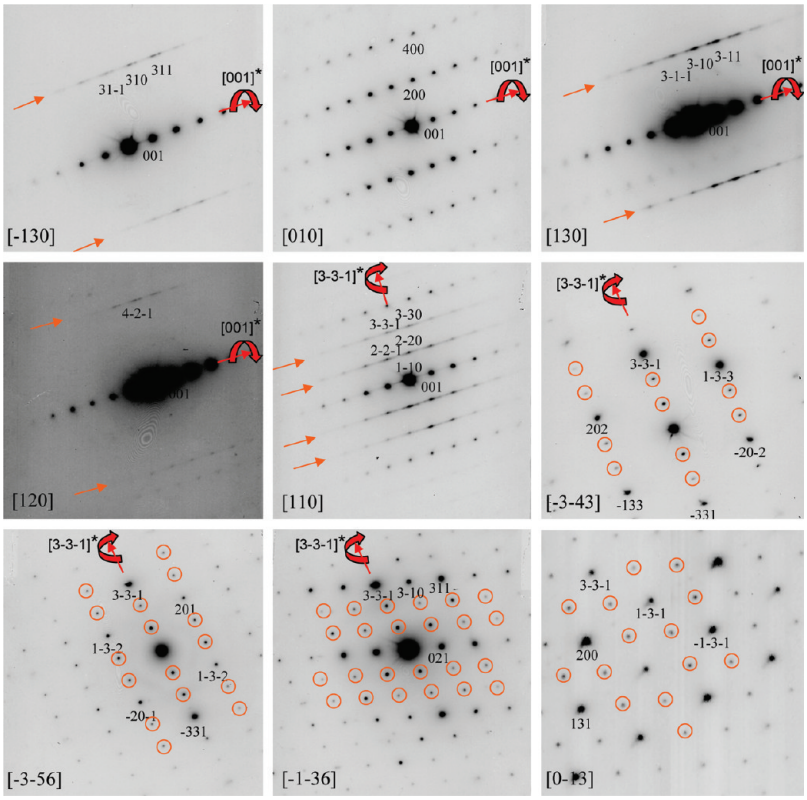

Figure 2. Electron diffraction patterns of the as prepared Li_2MnO_3 sample indexed in the $C2/m$ space group. Arrows indicate the location of diffuse scattering lines, and the circles highlight the extra spots which cannot be indexed in the $C2/m$ space group.

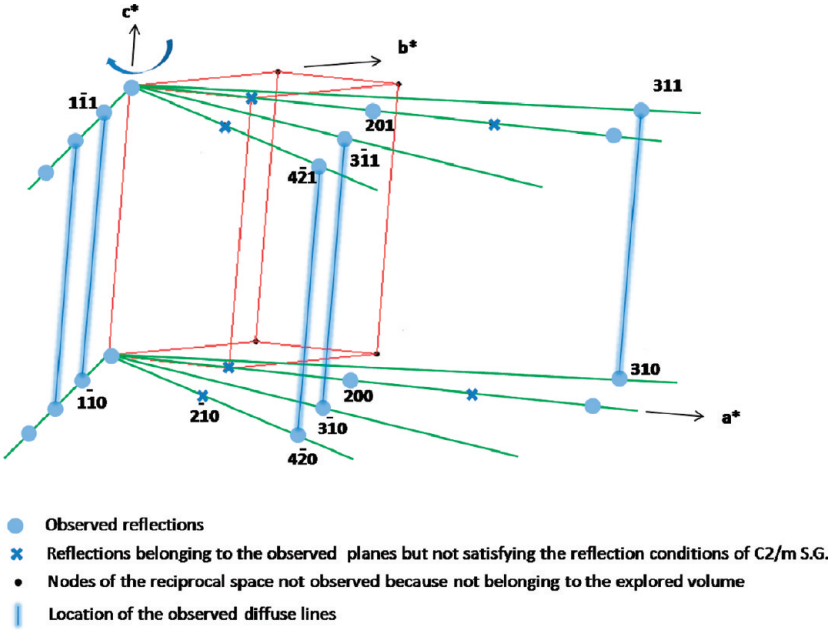

Figure 3. Three dimensional arrangement of the diffuse scattering lines along the c^* direction using the first five electron diffraction patterns reported in Figure 2.

planes that cannot be indexed with the trigonal cell, it means that diffusion is linked to some kind of disorder appearing in the stacking of the ordered cationic ($Li_{1/3}Mn_{2/3}$) planes. Such a condition of scattering lines existence is consistent with an *ab ca bc* faulted slabs stacking of a close packed array, [27] and this is in perfect accordance with the selective bottom broadening of the superstructure peaks observed in the XRD pattern mentioned above (Figure 1).

Among the presence of these diffuse scattering lines, additional spots are also observed in almost all the other

(27) Guinier, A. *Théorie et technique de la radiocristallographie*, 3rd ed.; Dunod: Paris, 1964; p 554.

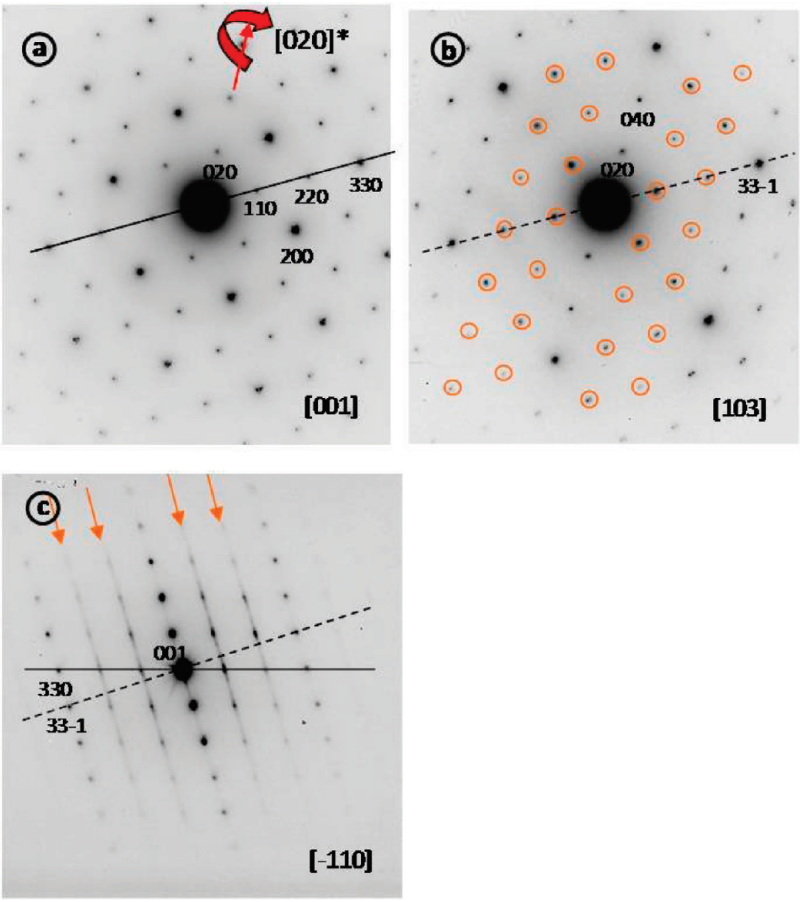

Figure 4. [001], [103], and [$\bar{1}$10] zone axis electron diffraction patterns. The arrows indicate the location of diffuse scattering lines, and the circles indicate spots that are due to the interception of the streakings with the Ewald's sphere.

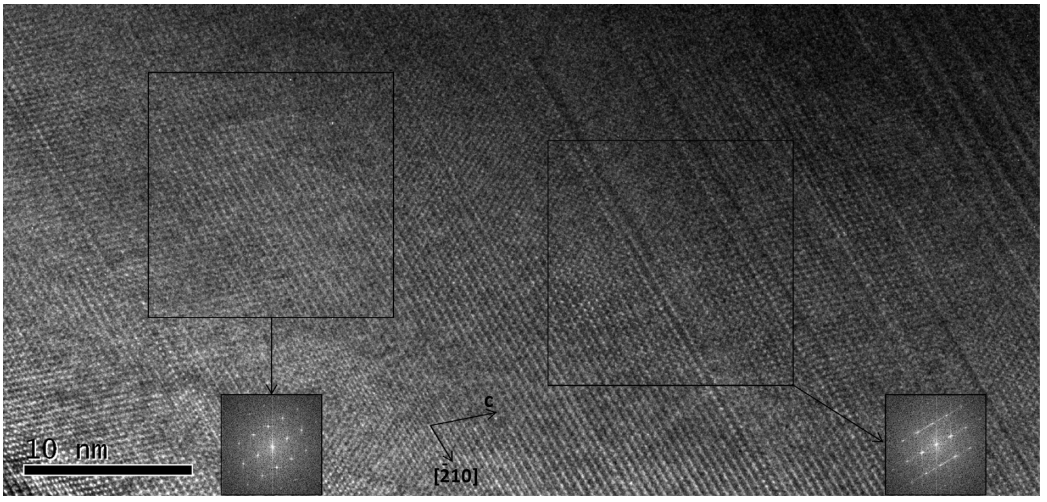

Figure 5. High resolution image obtained on a crystal oriented along the [110] monoclinic zone axis. The Fourier transforms was calculated for a faulted area of the crystal and for a perfect stacked part for comparison.

patterns which do not contain the c^* axis. As a matter of fact, on the four last patterns of Figure 2, that is, the [$\bar{3}$43], [$\bar{3}$56], [$\bar{1}$36], and [0$\bar{1}$3] zone axis patterns, only the main reflections can be indexed in the monoclinic cell. Additional reflections, circled on the patterns, appear. To understand the origin of these extra reflections, let us consider Figure 4. The [103] zone axis pattern (Figure 4b) is deduced from the [001] (Figure 4a) by rotation around the [020]* direction. On the [001] zone axis pattern, all the reflections are indexed in the $C2/m$ space group, whereas additional reflections (circled in red on Figure 4b), are observed in the second pattern. For instance, between the origin and the 33$\bar{1}$ reflection two additional spots are clearly observed. To understand this, it is necessary to observe the plane of the reciprocal space that contains the spots 33$\bar{1}$, 330, and 001, because diffuse scattering lines

are along c^*; this plane of the reciprocal space is the $[\bar{1}10]$ zone axis pattern; see Figure 4c. Diffuse scattering lines are observed on this pattern. On the $[\bar{1}10]$ zone axis pattern (Figure 4c), the solid line (respectively dotted line) indicates its intersection with the [001] zone axis pattern (respectively [103] zone axis pattern). The solid line links the transmitted and the 330 spots by *passing* via the spots 110 and 220, while the dotted one links the transmitted spot and the $33\bar{1}$ by *crossing* the diffuse scattering line. Thus, the extra spots observed in the [103] zone axis pattern are due to the intersection of the diffuse scattering lines with the Ewald's sphere, while there are no extra spots in the [001] zone axis pattern.

Meng et al. already obtained electron diffraction patterns of Li_2MnO_3 (Figures 10a and 10d in ref 23). Our own patterns are fully consistent with these experimental data. Even more, our Figure 4b and Figure 10d of ref 23 can be directly compared; they represent the same reciprocal plane. Nevertheless, our interpretation based on the existence of the diffuse scattering lines differs from that of Meng et al. who explained the same pattern using a superstructure. Note that our 3D reinvestigation of the reciprocal space does not show the existence of such a superstructure. Indeed, we have demonstrated that this diffraction patterns can be fully interpreted with the $C2/m$ space group and the diffuse scattering lines we pointed out. Note also that in the same paper, Meng et al. observed the same additional spots for the $Li[Ni_{1/2}Mn_{1/2}]O_2$ compound that they also interpreted as a superstructure of the parent trigonal structure. For this compound they have evidenced diffusion lines which are located exactly as in our study of Li_2MnO_3, but their consequence on the other patterns has not been considered.

3.3. High Resolution Transmission Electron Microscopy Study. High resolution transmission electron microscopy has been used to evidence such faults consisting of the random stacking of the cationic ordered ($Li_{1/3}Mn_{2/3}$) planes. A part of a crystal of the preparation is presented in Figure 5. Note that this crystal is representative of the whole material. It is oriented along the [110] zone axis and presents areas of perfectly stacked slabs separated by defects. Indeed this is confirmed by the fast Fourier transforms (FFTs) of the image, which can be considered as calculated electron diffraction patterns. The FFT calculated in the defect free part of the crystal shows no diffusion, whereas that calculated in an area with faults reveals the presence of diffuse scattering lines. The images obtained on larger areas show a nonhomogeneous distribution of the stacking faults. Some large parts of the crystals are perfect, while in other parts of the crystal, the frequency of the defects is very high. This is consistent with the conclusion of Breger et al. [22] as well as with our results obtained fom X-ray diffraction patterns simulations and reported in ref 24; that is, the stacking faults are gathered in some part of the crystals. An image taken from another crystal of the same preparation is shown in Figure 6a. The higher magnification allows details to be distinguished. A unique

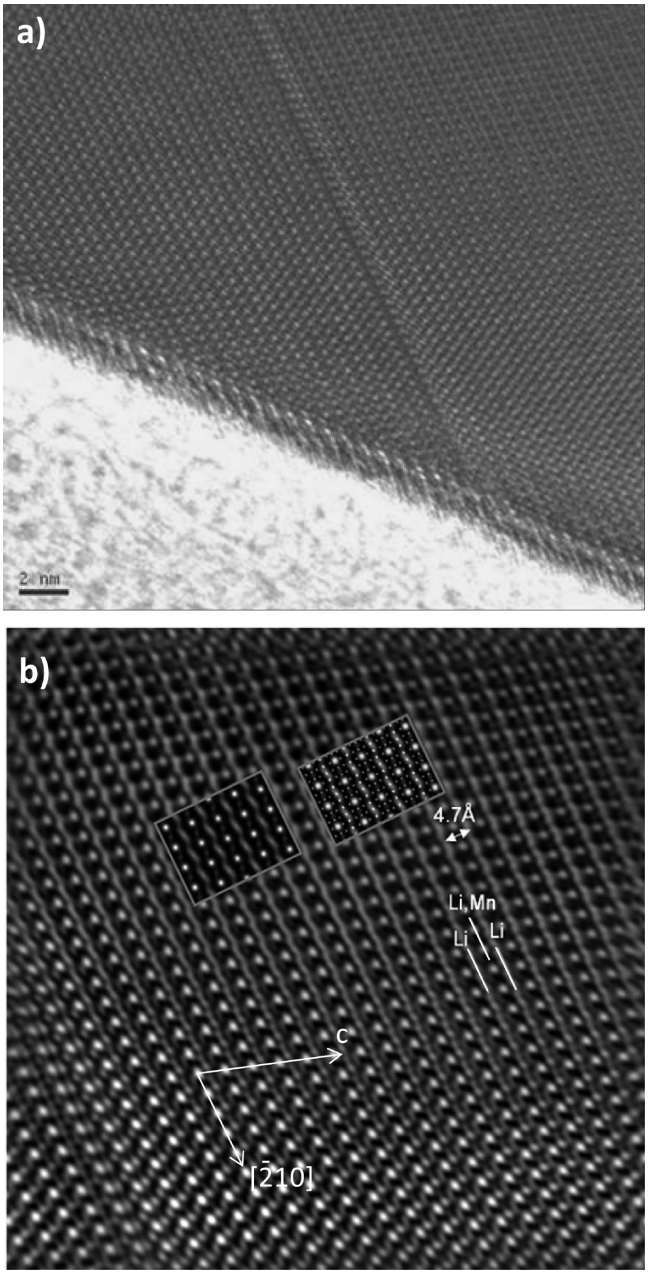

Figure 6. High resolution image observed along the [110] monoclinic zone axis. (a) Image of one stacking fault separating two ideal stacked areas, and (b) detail of a perfect part of the crystal; the corresponding simulated image (Δf = 43 nm and t = 39 nm) is shown in the center, and the atomic stacking seen along the same direction is in the inset.

fault running across the crystal, which is perfect elsewhere, can be seen. The perfect right part of the image could be simulated using the structural parameters calculated from the X-ray diffraction data; see Figure 6b. The condition of the simulation (defocus (Δf) and thickness of the specimen (t) were chosen from a matrix of simulated images (see Figure S1 given in the Supporting Information).

Finally, the influence of a stacking fault on a high resolution image has been studied. The aim was to compare a typical experimental image highlighting a faulted stacking of the slabs along the stacking axis with a simulated one. The effect of a stacking fault was

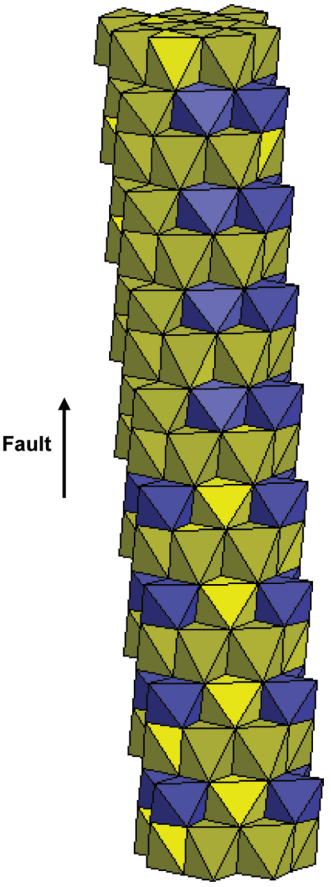

Figure 7. Schematic representation of the stacking sequence used to simulate the influence of a stacking fault diluted among well stacked slabs.The yellow octahedra contain lithium atoms and the blue ones manganese atoms.

simulated using a cell constituted by a fault diluted among a series of well stacked slabs. The fault is induced by the occurrence of the stacking vector (1/6; −1/6; 1) instead of the ideal one (0; 0; 1) in the monoclinic description. The stacking sequence used is represented in Figure 7. Therefore, an image simulation could be performed considering this slab stacking sequence seen along the [110] zone axis in the monoclinic description. A typical representative high resolution image collected with the synthesized powder is given in Figure 8a and compared to the simulated one in Figure 8b. Experimental and theoretical faulted images are very similar, and as evidenced by the line drawn, the created fault produces, as observed experimentally, a displacement of the atomic lines where the fault is localized; see Figure 8a. The locations of the faults are marked by arrows on each image. This simulation illustrates the fact that the stacking faults experimentally observed can be unequivocally related to the gliding of some slabs along the vectors of coordinates (1/6; −1/6) or (1/2; −1/6) in the (*a*; *b*) plane in the monoclinic system.

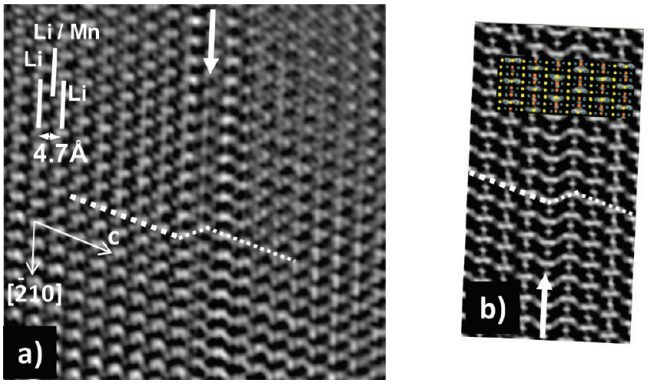

Figure 8. Comparison of an experimental image, along the [110] monoclinic zone axis, showing a stacking fault in (a) with a simulated one in (b). The locations of the faults are materialized by arrows, and the broken lines represent the succession of the atomic columns that are broken by the fault.

4. Conclusion

The aim of this study was to give a better understanding of the crystallographic properties of the Li_2MnO_3 compound.

The occurrence of the diffuse scattering lines is due to a faulted (or random, in the worse case) stacking of the ordered ($Li_{1/3}Mn_{2/3}$) cationic planes along the *c* axis. The relationship between the XRD patterns and the electron diffraction ones has been shown, highlighting that controversies existing in literature about the structure of Li_2MnO_3 have a common origin and are in fact related to cationic stacking faults that have been illustrated for the first time in such materials by the means of high resolution transmission electron microscopy images.

Reflections that cannot be explained in the *C*2/*m* space group are observed in the electron diffraction patterns of Li_2MnO_3. Our complete investigation of the reciprocal space demonstrates that diffuse scattering lines, parallel to the *c** monoclinic axis and running through the nodes which are characteristic of the monoclinic symmetry, do exist. The intersection of these diffuse scattering lines with the Ewald's sphere is, in fact, responsible for the observation of extra spots in the reciprocal space: no superstructure is thus needed for their interpretation.

Acknowledgment. The authors thank Région Aquitaine and the Ministère de l'Enseignement Supérieur et de la Recherche for their financial support.

Supporting Information Available: Matrix of of simulated high resolution images calculated for fault free Li_2MnO_3 considering various defocuses (*f*) and specimen thicknesses (*t*) and refined structural and profile parameters for Li_2MnO_3 (PDF). This material is available free of charge via the Internet at http://pubs.acs.org.